

Second harmonic generation spectroscopy on second harmonic resonant plasmonic metamaterials

HEIKO LINNENBANK AND STEFAN LINDEN*

Physikalisches Institut, Rheinische Friedrich-Wilhelms Universität Bonn, 53115 Bonn, Germany

*Corresponding author: linden@physik.uni-bonn.de

Received 5 May 2015; revised 25 June 2015; accepted 27 June 2015 (Doc. ID 240329); published 4 August 2015

The field enhancement resulting from the resonant excitation of plasmonic modes in metallic nanostructures allows to amplify nonlinear processes such as second harmonic generation in plasmonic metamaterials. Thus far, nonlinear experiments with metallic nanostructures relied on the resonant enhancement of the pump light by a plasmonic mode. Here, we report on second harmonic generation spectroscopy on plasmonic metamaterials that only exhibit a plasmonic resonance at twice the pump frequency. We also observe in this case a strong enhancement of the second harmonic generation signal, even though the driving pump field is not resonantly enhanced. The experimental data can be explained in terms of the anharmonic oscillator model and classical symmetry selection rules applied to nonlinear metamaterials. Our findings pave the way for further optimizations of the nonlinear response of plasmonic metamaterials. © 2015 Optical Society of America

OCIS codes: (160.3918) Metamaterials; (160.4330) Nonlinear optical materials; (190.2620) Harmonic generation and mixing; (310.6628) Subwavelength structures, nanostructures.

<http://dx.doi.org/10.1364/OPTICA.2.000698>

Second harmonic generation (SHG), the instantaneous conversion of a strong pump wave into a new wave with twice the frequency inside a material lacking inversion symmetry, was the first nonlinear optical process observed [1], roughly one year after the first demonstration of the laser. In an early study on SHG in piezoelectric crystals, R. C. Miller found the unexpected result that even though the second-order polarization coefficients of different crystals vary by several orders of magnitude, the ratio of the respective nonlinear coefficient and the product of the first-order susceptibilities of the same material at the pump frequency and the second-harmonic (SH) frequency is roughly constant [2]. This empirical correlation was subsequently theoretically justified in the framework of an anharmonic oscillator model and is now known as Miller's law [3].

An interesting consequence of this correlation is an enhancement of the second-order nonlinear susceptibility in the case that the linear susceptibility exhibits a resonance at either the pump or the SH frequency [4]. While an enhancement of the second-order nonlinear susceptibility is, of course, desirable for achieving high conversion efficiencies, both effects are not commonly used in bulk materials due to the associated strong absorption of either the pump or the generated SH light field [5,6].

However, the situation is different for SHG from thin films and surfaces, as in these cases propagation effects play a minor role. For instance, a remarkable amount of research has been carried out on SHG from plasmonic metamaterials, man-made effective materials consisting of noble metal nanostructures with tailored localized plasmon modes [7,8]. Here, the resonant excitation of localized plasmon modes gives rise to a concentration of the incident electromagnetic field in the vicinity of the metal nanostructures. As a result, the local intensity can exceed the incident intensity by orders of magnitude. Due to this concentration of the incident field, i.e., the pump field, nonlinear optical processes like SHG can be strongly enhanced. Based on this approach, SHG from different plasmonic nanostructures has been experimentally studied [9–13]. The SHG efficiency of plasmonic metamaterials can be further improved, e.g., by adding passive plasmonic elements to a metamaterial [14] or by optimizing the density of the plasmonic nanostructures in the metamaterial [15].

Another promising approach is based on a doubly resonant configuration in which plasmonic nanostructures are employed that are resonant to *both* the driving pump field and the SH signal [16–18]. In this scheme, the plasmonic mode resonant to the pump field amplifies the nonlinear conversion (see above), whereas the plasmonic mode resonant to the SHG signal is assumed to efficiently radiate the generated light to the far field. In contrast to this, SHG spectroscopy on doubly resonant split ring resonator arrays showed that resonances at the SH frequency can potentially also act as a loss channel [19].

In all previous experiments on doubly resonant metallic nanostructures, the nonlinear response has been dominated by the plasmonic resonance for the pump wave. This makes it difficult to exactly specify the influence of the plasmonic resonance at the SH frequency on the dispersion of the SHG efficiency. An earlier

study on SHG from silver nanoisland films with varying volumes using a fixed pump frequency indicated that an enhancement due to a plasmonic resonance at the SH frequency only is achievable [20]. Effects related to the changes of the plasmon resonance frequency and effects resulting from variations of the silver island film morphology were, however, not clearly distinguished in that work, which hampers the interpretation of these data. Moreover, due to the use of a fixed pump frequency, the dispersion of the SHG efficiency could not be determined.

In this Letter, we perform SHG spectroscopy on metamaterials consisting of lithographically defined noncentrosymmetric gold nanostructures that are solely resonant to the SH frequency in order to clearly identify the effect of a plasmonic mode at the SH frequency on the dispersion of the SHG efficiency. We observe a strong enhancement of the SHG signal at the plasmonic resonance frequency, even though the incident pump field is not resonantly enhanced. The dispersion as well as the polarization properties of the SHG spectra can be explained by the anharmonic oscillator model [21] and the measured linear extinction spectra in combination with the classical symmetry selection rules for dipolar SHG. This finding is a strong indication that the plasmonic mode at the SH frequency resonantly enhances the second-order nonlinear susceptibility and hence plays an active role in the SHG process.

For our investigations, we used V-shaped gold nanostructures with two different arm lengths of 90 and 140 nm, respectively. All nanostructures have an arm width and height of 40 nm and are arranged on a 300 nm × 300 nm square lattice with a footprint of 70 μm × 70 μm. The gold nanostructures were fabricated by standard electron-beam lithography and lift-off techniques on the same 0.5 mm thick borosilicate glass substrate covered with a 10 nm thin film of indium-tin oxide (ITO) as a conduction and adhesion layer. Scanning electron microscope (SEM) micrographs of both arrays are shown in Fig. 1. We have chosen this type of nanostructure for our investigation because it is noncentrosymmetric and hence should render possible dipolar SHG [21]. Furthermore, the linear optical properties of the V-shaped nanostructures are well understood [14]. They exhibit plasmonic resonances at distinct wavelengths for distinct polarizations.

The linear extinction (one minus transmission) spectra of the nanostructure arrays were measured by recording the transmitted intensity of the polarized white light delivered by a halogen lamp through the nanostructure arrays under normal incidence with a sandwich Si/InGaAs photodiode coupled to a monochromator. All spectra were normalized to reference spectra taken on the bare ITO-covered glass substrate.

As the pump light source for SHG spectroscopy, we employed a double-pass optical parametric generator (OPG) delivering pulses with a length of 200–300 fs (spectral FWHM: 8–40 nm) at a 42 MHz repetition rate tunable from 1400 to 1680 nm [22]. The average power of the pump beam was attenuated to 50 mW, and its linear polarization was controlled by the combination of a polarizer and an achromatic half-wave plate. The pump light was focused down to an approximately 30 μm spot diameter under normal incidence with an $f = 50$ mm plano-convex lens, resulting in an effective numerical aperture of less than 0.1. The SHG signal transmitted through the glass substrate was collected with a similar lens, separated from the residual pump light with a dichroic mirror, and recorded with a CCD spectrometer for different pump wavelengths in steps of approximately 10 nm. Additionally, a removable polarizer could be used to characterize

the polarization of the SH light. In order to eliminate any parasitic effects due to changes in the pulse shape and beam divergence when tuning the OPG, a reliable reference is required. In a reference arm, accessible via removable mirrors, the p -polarized pump beam is focused, under the same conditions as in the measurement arm, on the surface of a z -cut quartz plate under 45° incidence. An aperture in front of the collecting lens blocks all SH light originating from the volume of the quartz plate in order to record only the surface SHG signal, whose efficiency is, for our tuning range, wavelength independent [19]. For each pump wavelength, the spectrally integrated SHG signals from the nanostructure arrays were referenced to the spectrally integrated SHG signals from the reference arm. As similar pump power and optics were used in both arms, the given referenced SHG signals from the nanostructure arrays can thus be directly compared to each other.

Before we address the experimental results, we want to discuss the anticipated polarization properties of the SHG signal. As we perform the excitation under normal incidence with rather weak focusing, the polarization component of the pump light in the z direction can be neglected. Due to the symmetry of the V-shaped nanostructures, the following five elements of the second-order nonlinear susceptibility for SHG χ_{ijk}^{SHG} should be nonvanishing in dipolar approximation [23]: $\chi_{xxy}^{\text{SHG}} = \chi_{xyx}^{\text{SHG}}$, χ_{yxx}^{SHG} , χ_{yyy}^{SHG} , and χ_{zxx}^{SHG} . Here, the indices x , y , and z refer to the Cartesian coordinates (see Fig. 1). For our experimental conditions, the last element can be discarded, since the corresponding SHG signal is not emitted in the forward direction. The different tensor elements can be separated by evaluating the SHG signal as a function of both the polarization of the pump light and the polarization of the SH light [23].

The dispersion of the individual tensor elements χ_{ijk}^{SHG} can be understood in the following way. According to the anharmonic oscillator model, the second-order nonlinear susceptibility for SHG χ_{ijk}^{SHG} can be expressed by the linear susceptibilities χ_{ii} at the frequencies ω and 2ω :

$$\frac{\chi_{ijk}^{\text{SHG}}(2\omega, \omega, \omega)}{\chi_{ii}(2\omega)\chi_{jj}(\omega)\chi_{kk}(\omega)} = \frac{m\epsilon_0^2 a_{ijk}}{N^2 e^3}. \quad (1)$$

Here, m denotes the electron mass and N the electron number density. The nonlinear restoring force is characterized by a_{ijk} [21]. Furthermore, the coordinate system was chosen such that the linear susceptibility is a diagonal tensor.

Figure 2(a) depicts the measured linear optical extinction spectra of the array of the small V-shaped structures for x and y polarization (black curves). The small Vs exhibit a strong plasmonic resonance for x -polarized light centered at around 800 nm wavelength, whereas no resonance for y -polarized light is observable

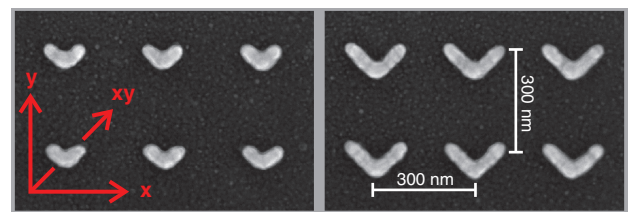


Fig. 1. Top-view SEM micrographs of 900 nm × 600 nm sections from the arrays of the two different-sized V-shaped nanostructures. The red arrows indicate the distinct linear polarizations used in this Letter.

within the spectral range relevant for this work (700–1680 nm). Obviously, the Vs show no plasmonic resonance within the tuning range of the pump source (1400–1680 nm). Thus, according to Eq. (1), we do not expect an enhancement of the second-order nonlinear susceptibility for SHG due to a resonant enhancement of the linear susceptibility at the pump light frequency. In contrast, the plasmonic resonance at around an 800 nm wavelength should lead to an enhancement of the $\chi_{xxy}^{\text{SHG}} = \chi_{xyx}^{\text{SHG}}$ elements due to a resonant enhancement of the linear susceptibility at the SH frequency. To test this expectation, we measured the total (i.e., polarization-unselective detection) SHG signal as function of the linear pump polarization direction at a pump wavelength of 1600 nm [see Fig. 2(b)]. As anticipated, the SHG signal is strongest for xy - and yx -polarized pump light. The slight asymmetry is probably related to fabrication imperfections. Figure 2(c) shows the polarization of the SH light for xy -polarized pump light at a pump wavelength of 1600 nm. We find that the SHG signal is clearly polarized along the x axis. This identifies the χ_{xxy}^{SHG} element as the dominant contribution to the second-order nonlinearity. By performing SHG spectroscopy with xy -polarized pump light on the array of small Vs [gray dots in Fig. 2(a)], we find, as expected, that the SHG efficiency closely follows the plasmonic resonance centered at around an 800 nm wavelength.

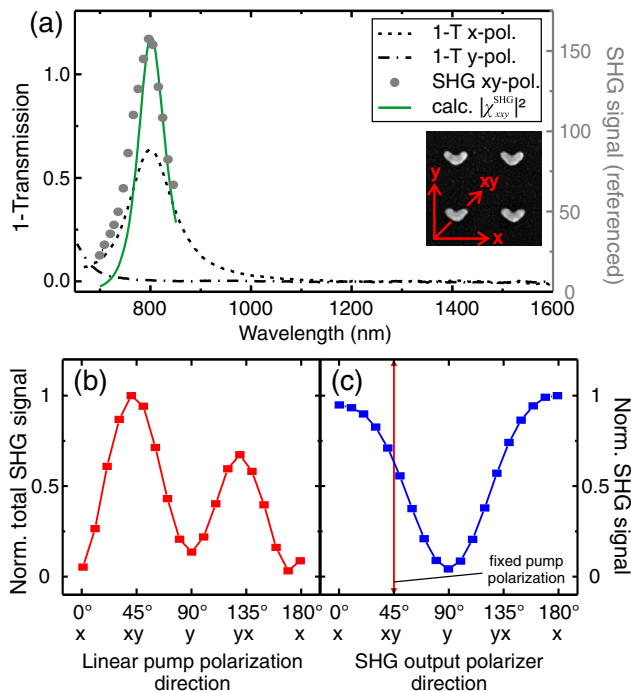


Fig. 2. (a) Left axis: normal-incidence optical extinction spectra of the array of small V-shaped plasmonic nanostructures for x - (dashed-dotted curve) and y - (dashed curve) incident polarization. Right axis: measured referenced SHG signal (dots) obtained with xy -polarized pump light and calculated $|\chi_{xxy}^{\text{SHG}}|^2$ (solid green curve) as a function of the SH wavelength. (b) Corresponding total SHG signal as a function of the angle of polarization of the linearly polarized incident pump beam and (c) corresponding SHG signal as a function of the linear output polarizer, at a pump wavelength of 1600 nm. The red vertical lines indicate the fixed linear polarization of the pump light. All data points in (b) and (c) are normalized to the maximum of each individual measurement [(b) 157 \times and (c) 135 \times SHG signal from the quartz reference] and connected as a guide to the eye.

The anharmonic oscillator model can be used to calculate the dispersion of the SHG signal. For this purpose, we assume that the linear extinction for linear polarized light along the i axis can be written as $1 - T_i(\omega) \approx \frac{\omega}{c} \Im[\chi_{ii}(\omega)]$ and that the linear susceptibility $\chi_{ii}(\omega)$ can be modeled with a single harmonic oscillator [21]. The parameters describing the harmonic oscillator, i.e., the resonance frequency, the damping, and the amplitude, and thus the linear susceptibility $\chi_{ii}(\omega)$, are obtained by fitting a Lorentzian to $\Im[\chi_{ii}(\omega)]$. Using Eq. (1), we find that $\chi_{ijk}^{\text{SHG}}(2\omega, \omega, \omega) \propto \chi_{ii}(2\omega)\chi_{jj}(\omega)\chi_{kk}(\omega)$. For a given polarization combination ijk , $|\chi_{ijk}^{\text{SHG}}(2\omega, \omega, \omega)|^2$ is proportional to the corresponding referenced SHG signal. In the case of the small Vs, the constant of proportionality is chosen such that the maximum of the calculated $|\chi_{xxy}^{\text{SHG}}(2\omega, \omega, \omega)|^2$ matches the maximum of the measured referenced SHG signal [see Fig. 2(a), green curve]. Obviously, the measured dispersion of the SHG signal can be described well with the anharmonic oscillator model.

The measured linear optical extinction spectra of the array of the big V-shaped structures for x and y polarization are presented in Fig. 3(a) (black curves). Compared to the small Vs, the plasmonic resonance of the big Vs for x -polarized light is shifted to a wavelength of 1100 nm. Additionally, a plasmonic resonance for y -polarized light appears at a 740 nm wavelength. According to

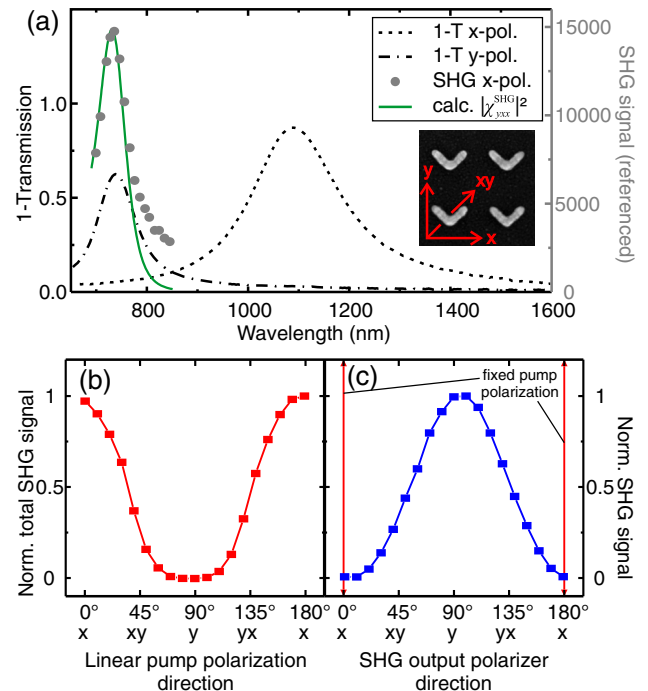


Fig. 3. (a) Left axis: normal-incidence optical extinction spectra of the array of big V-shaped plasmonic nanostructures for x - (dashed-dotted curve) and y - (dashed curve) incident polarization. Right axis: measured referenced SHG signal (dots) obtained with x -polarized pump light and calculated $|\chi_{yxx}^{\text{SHG}}|^2$ (solid green curve) as a function of the SH wavelength. (b) Corresponding total SHG signal as a function of the angle of polarization of the linearly polarized incident pump beam and (c) corresponding SHG signal as a function of the linear output polarizer, at a pump wavelength of 1480 nm. The red vertical lines indicate the fixed linear polarization of the pump light. All data points in (b) and (c) are normalized to the maximum of each individual measurement [(b) 14763 \times and (c) 13405 \times SHG signal from the quartz reference] and connected as a guide to the eye.

Eq. (1), an enhancement of both elements χ_{yxx}^{SHG} and χ_{yyy}^{SHG} due to a plasmonic resonance at the SH frequency for y -polarized light can be expected. In contrast, no enhancement of the elements $\chi_{xxy}^{\text{SHG}} = \chi_{xyx}^{\text{SHG}}$ is anticipated, since the big Vs have no plasmonic resonance at either the pump frequency or the SH frequency for x -polarized light. A measurement of the total SHG signal as a function of the linear pump polarization direction at a pump wavelength of 1480 nm [see Fig. 3(b)] yields a strong SHG signal for x -polarized pump light only. Figure 3(c) shows that the SH light is linearly polarized in the y direction for a fixed polarization of the pump light in the x direction and a pump wavelength of 1480 nm. These experiments demonstrate that for the big Vs, the element χ_{yxx}^{SHG} yields the strongest contribution to the second-order nonlinearity, whereas the symmetry allowed element χ_{yyy}^{SHG} does not play a significant role. This finding can be explained by the influence of the tail of the plasmonic resonance centered at a 1100 nm wavelength, which provides an off-resonant contribution to the linear susceptibility $\chi_{xx}(\omega)$ at the pump frequency. The SHG spectroscopy data measured with x -polarized pump light [gray dots in Fig. 3(a)] show that the SHG efficiency closely follows the plasmonic resonance for y -polarized light. This indicates that the plasmonic resonance at the SH frequency governs the dispersion of the second-order nonlinear susceptibility. Finally, we compare the measured SHG signal with the calculated $|\chi_{yxx}^{\text{SHG}}|^2$ using the procedure described above. The corresponding data are shown in Fig. 3(a) (green curve). Again, we find very good agreement between experimental data and theory.

It is interesting to compare the maxima of the SHG signals of the two different arrays of Vs. Inspection of Figs. 2(a) and 3(a) show that the maximum SHG signal of the large Vs is approximately two orders larger than that of the small Vs. This cannot be explained by only the larger amount of gold, which enters Eq. (1) via the electron number density N . Rather, we have to keep in mind that in the case of the large Vs we have a noticeable off-resonant contribution of the plasmonic resonance at a wavelength of 1100 nm to the linear susceptibility at the pump frequency (see discussion of Fig. 3), while in the case of the small Vs, the second-order nonlinear susceptibility is only enhanced by a plasmonic resonance for the SH frequency.

In conclusion, we have demonstrated that the SHG efficiency of metamaterials can be enhanced, exploiting nanostructures that solely exhibit a resonance for the SH light. SHG spectroscopy was used to resolve the influence of a plasmonic resonance at the SH frequency on the dispersion of the SHG efficiency. Our findings show that the SHG response of plasmonic metamaterials can be well understood by the help of the anharmonic oscillator model and the knowledge of the linear extinction spectra. In this model, the plasmonic resonance at the SH frequency does not merely act as a passive element that helps to efficiently radiate the SH light to the far field but also plays an active role in the SHG process. Furthermore, our experiments provide a strong indication that

the classical symmetry selection rules for dipolar SHG are valid for plasmonic nanostructures. We are convinced that our findings can be used to further optimize the nonlinear response of plasmonic metamaterials.

Note: We have recently become aware of a related study on the enhancement of second harmonic emission by plasmonic resonances of aluminum nanoantennas at the second harmonic wavelength [24].

Funding. Deutsche Forschungsgemeinschaft (DFG) (SPP1391).

REFERENCES

1. P. A. Franken, A. E. Hill, C. W. Peters, and G. Weinreich, *Phys. Rev. Lett.* **7**, 118 (1961).
2. R. C. Miller, *Appl. Phys. Lett.* **5**, 17 (1964).
3. C. Garrett and F. Robinson, *IEEE J. Quantum Electron.* **2**, 328 (1966).
4. W. Ettoumi, Y. Petit, J. Kasparian, and J.-P. Wolf, *Opt. Express* **18**, 6613 (2010).
5. R. Chang, J. Ducuing, and N. Bloembergen, *Phys. Rev. Lett.* **15**, 415 (1965).
6. R. L. Byer, *Ann. Rev. Mater. Sci.* **4**, 147 (1974).
7. P.-Y. Chen, C. Argyropoulos, and A. Alù, *Nanophotonics* **1**, 221 (2012).
8. M. Kauranen and A. V. Zayats, *Nat. Photonics* **6**, 737 (2012).
9. B. Lambrecht, A. Leitner, and F. Aussenegg, *Appl. Phys. B* **64**, 269 (1997).
10. B. K. Canfield, H. Husu, J. Laukkanen, B. Bai, M. Kuittinen, J. Turunen, and M. Kauranen, *Nano Lett.* **7**, 1251 (2007).
11. M. W. Klein, M. Wegener, N. Feth, and S. Linden, *Opt. Express* **15**, 5238 (2007).
12. F. B. Niesler, N. Feth, S. Linden, J. Niegemann, J. Gieseler, K. Busch, and M. Wegener, *Opt. Lett.* **34**, 1997 (2009).
13. M. J. Huttunen, G. Bautista, M. Decker, S. Linden, M. Wegener, and M. Kauranen, *Opt. Mater. Express* **1**, 46 (2011).
14. R. Czaplicki, H. Husu, R. Siikano, J. Mäkitalo, M. Kauranen, J. Laukkanen, J. Lehtolahti, and M. Kuittinen, *Phys. Rev. Lett.* **110**, 093902 (2013).
15. S. Linden, F. B. P. Niesler, J. Förstner, Y. Grynko, T. Meier, and M. Wegener, *Phys. Rev. Lett.* **109**, 015502 (2012).
16. K. Thyagarajan, S. Rivier, A. Lovera, and O. J. Martin, *Opt. Express* **20**, 12860 (2012).
17. M. Celebrano, X. Wu, M. Baselli, S. Grossmann, P. Biagioni, A. Locatelli, C. De Angelis, G. Cerullo, R. Osellame, B. Hecht, F. Ciccacci, and M. Finazzi, *Nat. Nanotechnol.* **10**, 412 (2015).
18. H. Aouani, M. Navarro-Cia, M. Rahmani, T. P. H. Sidiropoulos, M. Hong, R. F. Oulton, and S. A. Maier, *Nano Lett.* **12**, 4997 (2012).
19. F. B. P. Niesler, N. Feth, S. Linden, and M. Wegener, *Opt. Lett.* **36**, 1533 (2011).
20. A. Wokaun, J. G. Bergman, J. P. Heritage, A. M. Glass, P. F. Liao, and D. H. Olson, *Phys. Rev. B* **24**, 849 (1981).
21. F. Hopf and G. Stegeman, *Applied Classical Electrodynamics, Volume II: Nonlinear Optics* (Wiley, 1986).
22. H. Linnenbank and S. Linden, *Opt. Express* **22**, 18072 (2014).
23. Y. Zeng, W. Hoyer, J. Liu, S. Koch, and J. Moloney, *Phys. Rev. B* **79**, 235109 (2009).
24. B. Metzger, L. Gui, J. Fuchs, D. Floess, M. Hentschel, and H. Giessen, *Nano Lett.* **15**, 3917 (2015).